A series approach to wetting and layering transitions. III. The chiral clock model

1988 J. Phys. A: Math. Gen. 21 173

(http://iopscience.iop.org/0305-4470/21/1/023)

J. Phys. A: Math. Gen. 21 (1988) 173-195. Printed in the UK

A series approach to wetting and layering transitions: III. The chiral clock model

K Armitstead and J M Yeomans

Department of Theoretical Physics, University of Oxford, 1 Keble Road, Oxford OX1 3NP, UK

Received 11 May 1987

Abstract. In the third of this triad of papers which study interfacial phase transitions using series expansions we treat the wetting transition of an interface in the three-state chiral clock model. Previous work has shown that on a simple cubic lattice at low temperatures the interface wets through a large, possibly infinite, number of layering transitions. We extend the low-temperature series results to an arbitrary number of nearest neighbours and show that, in the mean-field limit of infinite coordination number, only two layering transitions are seen. This is in agreement with numerical solutions of mean-field equations. Hence the mean-field approximation in this case does not provide a correct description of interface behaviour in three dimensions.

1. Introduction

In this, the last of three papers on the application of series expansions to interface problems, we study the wetting of an interface in the three-dimensional, three-state, chiral clock model. This extends previous work (Armitstead *et al* 1986), the results of which are summarised below. The model comprises three equivalent states with the wetting transition occurring when one of the coexisting phases intrudes at a boundary between the other two. The wetting layer therefore has two interfaces, both of which may fluctuate, in contrast to the semi-infinite systems studied in the first two papers of this series (Armitstead and Yeomans 1987, 1988), where one of the interfaces is replaced by a rigid wall. This makes the calculations more complex, but the same approaches—low-temperature series and mean-field theory—are still applicable. Our particular aim in this paper is to compare the two approximations and show that the results obtained from the low-temperature series for a three-dimensional simple cubic lattice differ from those resulting from the use of mean-field theory.

The rest of the introduction is devoted to a description of the chiral clock model and a summary of the results obtained previously from a low-temperature expansion (Armitstead *et al* 1986). Section 2 describes how the mean-field equations of the model can be set up and solved numerically. This gives a qualitatively different phase diagram from the low-temperature series. The discrepancy is resolved in § 3 where the low-temperature expansion is generalised to allow for an arbitrary number of nearest neighbours. Taking the coordination number to infinity gives a low-temperature analytical approximation to the mean-field equations (Szpilka and Fisher 1986), the results of which agree with those obtained numerically. The analytic approach allows us to show that mean-field theory predicts the wrong phase diagram because it

0305-4470/88/010173+23$02.50

underestimates the fluctuations which lead to the layering transitions. In addition, we demonstrate how the phase diagram develops from the simple cubic case to the mean-field limit as the coordination number is increased. Finally, in § 4, we summarise the important results from both this and our earlier papers in the series (Armitstead and Yeomans 1987, 1988).

The three-state chiral clock model is defined by the Hamiltonian

$$H = -\tfrac{1}{2}J_0 \sum_{ijj'} \cos[2\pi(n_{i,j} - n_{i,j'})/3] - J \sum_{ij} \cos[2\pi(n_{i,j} - n_{i+1,j} + \Delta)/3] \tag{1.1}$$

where the variables $n_{i,j}$ are situated on each site of a cubic lattice and can take the values 0, 1, 2. i labels two-dimensional layers perpendicular to a given axial direction and j labels sites within each layer. Hence the first sum is taken over nearest neighbours within the layers, whereas the second is between nearest neighbours along the axial direction. At zero temperature the ordering within the layers is ferromagnetic, although the value of $n_{i,j}$ may vary from layer to layer: for $\Delta < \frac{1}{2}$ the ordering between layers is ferromagnetic; for $\Delta > \frac{1}{2}$, however, there is a chiral ground state, ... 012012012 ....

To study the interface properties of the three-state chiral clock model (Huse and Fisher 1984), we introduce an interface perpendicular to the axial direction by forcing the spins at $i = -\infty$ and $i = +\infty$ to take the values 0 and 2, respectively. This results in a 0:2 interface for sufficiently small Δ. As Δ is increased, however, the energy of a 0:1 interface (and equivalently 1:2 and 2:0) decreases, whereas that of a 0:2 interface increases. Hence it becomes favourable at a certain value, $\Delta = \frac{1}{4}$, for the interface to wet, and for the simple 0:2 interface to be replaced by the configuration 0:11 ... 11:2. Note that this is a purely energetic (zero-temperature) argument and that the number of layers, n, with $n_i = 1$, is arbitrary.

At finite temperatures entropy contributions will also be important. Armitstead *et al* (1986) used low-temperature series expansions to show that, for small temperatures near $\Delta = \frac{1}{4}$, the interface wets through a series of first-order layering transitions, with n increasing in integer steps as a function of Δ. The resulting interface phase diagram is shown in figure 1.

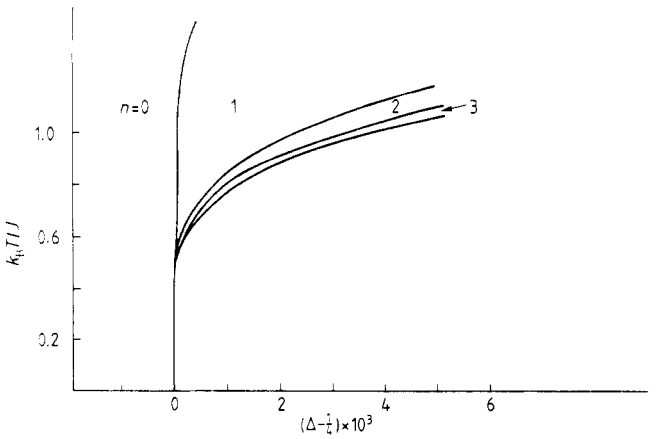

Figure 1. Interface phase diagram of the three-state chiral clock model on a simple cubic lattice, obtained from a low-temperature expansion.

The method used was analogous to that described in the first two papers of this series (Armitstead and Yeomans 1987, 1988). By establishing the leading-order terms which differentiate between the reduced free energies of interface phases n and $n' > n$, $F_n - F_{n'}$, the phase sequence could be built up inductively for successive values of n. One complication arose, however, because the usual chains of overturned axial spins of length n and their disconnections did not contribute to $F_{n'} - F_n$ to leading order. Hence axial chains of length $n+1$ and chains of length n with single side bumps also needed to be taken into account. The contribution from these could, however, be calculated using an extension of the matrix method introduced by Yeomans and Fisher (1984).

In § 3 of this paper the results of Armitstead *et al* (1986), which were for a simple cubic lattice, are extended to general coordination number. First, however, we derive and solve a mean-field theory for the three-state chiral clock model with an interface. We find that the results disagree with those obtained from low-temperature series.

2. Numerical mean-field theory

A mean-field theory for the three-state chiral clock model was first derived by Ottinger (1982), who analysed the bulk phase diagram. Although mean-field theory has inherent limitations in that it underestimates the effects of thermal fluctuations, the approximation usually leads to a qualitatively correct picture in three dimensions. However, Szpilka and Fisher (1986) have recently shown that this is not the case for the bulk properties of the three-state chiral clock model. Therefore, we now use a mean-field approximation to study the interface properties of the model to see if the layering transitions predicted by low-temperature series persist.

To derive the mean-field equations it is helpful to write the three spin states as two dimensional vectors, $\boldsymbol{S}$, which can take the values

$$\boldsymbol{S}^0 = \begin{pmatrix} 1 \\ 0 \end{pmatrix} \qquad \boldsymbol{S}^1 = \frac{1}{2}\begin{pmatrix} -1 \\ \sqrt{3} \end{pmatrix} \qquad \boldsymbol{S}^2 = \frac{1}{2}\begin{pmatrix} -1 \\ -\sqrt{3} \end{pmatrix} \tag{2.1}$$

and recast the Hamiltonian (1.1) in the form

$$H = -\tfrac{1}{2}J_0 \sum_{ijj'} \boldsymbol{S}_{i,j} \cdot \boldsymbol{S}_{i,j'} - J \sum_{ij} \boldsymbol{S}_{i,j} \cdot \mathbf{R}(-\Delta/3) \cdot \boldsymbol{S}_{i+1,j} \tag{2.2}$$

where

$$\mathbf{R}(\alpha) = \begin{pmatrix} \cos 2\pi\alpha & -\sin 2\pi\alpha \\ \sin 2\pi\alpha & \cos 2\pi\alpha \end{pmatrix}. \tag{2.3}$$

Using the Bogoliubov inequality as usual (Yokoi *et al* 1981, Ottinger 1982) gives for the mean-field free energy per spin, for a lattice of N layers,

$$F = \frac{1}{N}\sum_{i=1}^{N}\left[J\langle \boldsymbol{S}_i\rangle \cdot \mathbf{R}(-\Delta/3) \cdot \langle \boldsymbol{S}_{i+1}\rangle + 2J_0\langle \boldsymbol{S}_i\rangle \cdot \langle \boldsymbol{S}_i\rangle - k_B T \ln \sum_{k=0}^{2} \exp(H_i^k) \right] \tag{2.4}$$

where $\langle \boldsymbol{S}_i\rangle$ is the average spin in the ith layer. To introduce an interface into the system $\langle \boldsymbol{S}_1\rangle$ and $\langle \boldsymbol{S}_N\rangle$ were fixed to be equal to $\boldsymbol{S}^0$ and $\boldsymbol{S}^2$, respectively, and $\langle \boldsymbol{S}_{N+1}\rangle$ set equal to zero. $\langle \boldsymbol{S}_i\rangle$ was then determined for $2 \leq i \leq N-1$ by the self-consistency equations

$$\langle \boldsymbol{S}_i\rangle = \left(\sum_{k=0}^{2} \boldsymbol{S}^k \exp(H_i^k) \right)\left(\sum_{k=0}^{2} \exp(H_i^k) \right)^{-1} \tag{2.5}$$

with

$$H_i^k = \boldsymbol{S}^k \cdot \{J[\mathbf{R}(-\Delta/3) \cdot \langle \boldsymbol{S}_{i+1} \rangle + \mathbf{R}(\Delta/3) \cdot \langle \boldsymbol{S}_{i-1} \rangle] + 4J_0 \langle \boldsymbol{S}_i \rangle\} / k_B T. \tag{2.6}$$

The solutions to (2.5) were found by choosing an initial set of $\boldsymbol{S}_i$, $i = 2, \ldots, N-1$, and solving iteratively until self-consistency was achieved. The free energy of the resulting state was then calculated using (2.4). It is often possible to obtain many different solutions depending on the choice of initial conditions. The stable solution is that which corresponds to the absolute minimum of the free energy; the other solutions are local minima in the free energy, which may be interpreted as metastable states.

Once the stable solutions were obtained as a function of temperature and Δ, the transition could be most easily studied by measuring the excess fraction of spins in state $\boldsymbol{S}^1$ in each layer i, resulting from the presence of the interface, ΔS_i^1. Defining $\langle S_i^1 \rangle^{xy}$ to be the fraction of spins in layer i in state $\boldsymbol{S}^1$ with boundary conditions $\langle \boldsymbol{S}_1 \rangle = \boldsymbol{S}^x$ and $\langle \boldsymbol{S}_N \rangle = \boldsymbol{S}^y$, we may write

$$\Delta S_i^1 = \langle S_i^1 \rangle^{02} - \langle S_i^1 \rangle^{00}. \tag{2.7}$$

In figure 2 we show plots of ΔS_i^1 against, i, $1 \leqslant i \leqslant N = 20$, at $k_B T/J = 1.5$, $J = J_0$, for three values of Δ chosen so that phases $n = 0$, 1 and 6 (for the case $N = 20$) are stable. At this temperature these are the only phases observed. The magnitude of n in the final phase increased with the number of layers in the lattice, N; otherwise no quantitative differences in the results were seen as N was varied. Hence $n = 6$, for

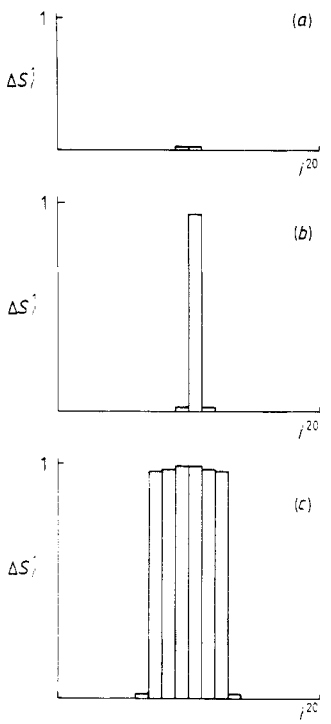

Figure 2. ΔS_i^1, the excess fraction of spins in state $\boldsymbol{S}^1$ per layer, as a function of i at $T = 1.5$ and (*a*) $\Delta = 0.250\,02$, (*b*) $\Delta = 0.250\,05$, (*c*) $\Delta = 0.26$.

$N = 20$, was interpreted as equivalent to $n = \infty$ in the thermodynamic limit: the interfaces moved as far away from one another as possible before being restricted by the size of the lattice. Therefore mean-field theory predicts only two transitions: $n = 0$ to 1, and $n = 1$ to ∞.

This phase picture persists up to $k_B T/J \approx 2.5$, above which the phase with $n = 2$ appears. However, the phase with $n = 3$ was not observed. At these temperatures the value of ΔS_i^1 was much reduced compared with those shown in figure 2, although there was still a significant increase over its value in the absence of the interface. This is to be expected because of thermal fluctuations. Because of these entropic effects, we were not able to confidently predict the phase diagram close to the bulk phase boundary. The phase diagram from these results is shown in figure 3. Note that, apart from the layering transitions which are obviously different from those in figure 1, the 0:1 boundary phase boundary, which has been exaggerated in $\Delta - \frac{1}{4}$ by a factor of 2 for clarity, shifts to a value below $\Delta = 0.25$ for $k_B T/J \gtrsim 2.25$. There is no evidence for this from the low-temperature series results.

It is not clear why mean-field theory should predict a different phase diagram—it is this question which we address in the next section. The change in behaviour at higher temperatures should be treated with caution, as it may be above roughening, which is neglected by mean-field theory.

3. Mean-field theory in the low-temperature approximation

We now extend the low-temperature series results of Armitstead *et al* (1986) to a lattice with an arbitrary number of nearest neighbours, $q_\parallel$ and $q_\perp$, parallel and perpendicular to the axial direction, respectively. In the limit $q_\perp, q_\parallel \to \infty$ with $q_\perp J_0$ and $q_\parallel J$ fixed, mean-field theory is exact (Thompson 1974, Szpilka and Fisher 1986). Our aim is to see how the results of the low-temperature series vary as this limit is approached. To show that the phase with $n = 2$ is not stable in mean-field theory, we need to consider terms up to third order in the series expansion. These calculations are outlined, leaving the details to appendix 1, in §§ 3.1, 3.2 and 3.3. In § 3.4 we show how to calculate the

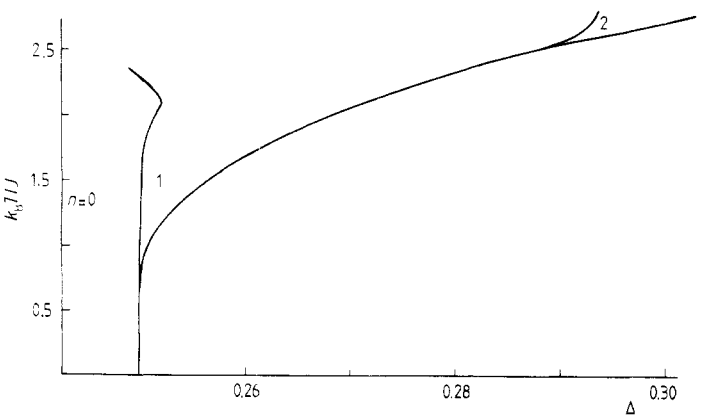

Figure 3. Interface phase diagram of the three-state chiral clock model from numerical mean-field theory. The kink in the 0:1 boundary is exaggerated by a factor of 2 in $\Delta - \frac{1}{4}$ for clarity.

leading term in the reduced free-energy difference at general order using a matrix method, which is further elucidated in appendix 2. This enables us to show how the phase diagram changes as the coordination number is increased, and to demonstrate that the sequence of phases in the mean-field limit is $n = 0, 1, \infty$.

First we introduce the notation for the primitive Boltzmann factors corresponding to single spin flips. It is useful to define

$$K_0 = J_0/k_B T \qquad K = J/k_B T \tag{3.1}$$

$$\delta = \Delta - \tfrac{1}{4} \qquad c = \cos(2\pi\delta/3) \qquad s = \sin(2\pi\delta/3) \tag{3.2}$$

where, as usual, k_B is Boltzmann's constant and T is the temperature. Then changing an in-layer bond from ferromagnetic to antiferromagnetic corresponds to a factor

$$w = \exp(-3K_0/2). \tag{3.3}$$

Two independent Boltzmann weights, x and y, are needed to describe the effect of altering an axial bond:

$$0\text{-}0 \to 0\text{-}1: \qquad x = \exp[(3s - \sqrt{3}c)K/2] \tag{3.4}$$

$$0\text{-}0 \to 0\text{-}2: \qquad y = \exp(-\sqrt{3}cK) \tag{3.5}$$

$$0\text{-}1 \to 0\text{-}2: \qquad x^{-1}y = \exp[(-3s - \sqrt{3}c)K/2]. \tag{3.6}$$

All other possibilities follow immediately from (3.4)-(3.6) when the symmetry of the Hamiltonian with respect to the different spin states is considered.

From (3.4)-(3.6) we may write

$$y = x^{2+\alpha} \tag{3.7}$$

where

$$\alpha \ln(x) = -3Ks. \tag{3.8}$$

This will be used in the calculations which follow, in order to expand y in terms of x when $y \approx x^2$.

Many of the details of the calculation follow those for the simple cubic lattice (Armitstead *et al* 1986) and similar expressions for the reduced free-energy differences are obtained. However, taking the mean-field limit causes different diagrams to dominate, and we shall therefore summarise the derivation of the equations to emphasise where the differences occur.

3.1. First order

Using the notation of § 1, let F_n be the reduced free energy per interface spin of a system with n layers of ones. It is convenient to introduce the notation

$$x^{q_\parallel/2} = \tilde{x} \qquad y^{q_\parallel/2} = \tilde{y} \qquad w^{q_\perp} = \tilde{w}. \tag{3.9}$$

Changing the coordination numbers $q_\parallel$ and $q_\perp$ whilst keeping $Kq_\parallel$ and $K_0 q_\perp$ constant leaves $\tilde{x}$, $\tilde{y}$ and $\tilde{w}$ unaltered.

From ground-state energies and single spin-flip excitations we obtain

$$F_1 - F_n = 2\tilde{x}^{-2}(\tilde{x}^2 - \tilde{y})(\tilde{x}\tilde{y} - 1)\tilde{w} + O(\tilde{w}^2 w^{-2}) \qquad n \geq 2 \tag{3.10}$$

$$F_0 - F_n = -3Ksq_\parallel/2 + (-2 + 2\tilde{x}^2\tilde{y}^{-1} + 4\tilde{x}\tilde{y} - 4\tilde{x}^{-1}\tilde{y}^2)\tilde{w} + O(\tilde{w}^2 w^{-2}) \qquad n \geq 2. \tag{3.11}$$

For

$$3Ksq_{\parallel}/2 \sim O(\tilde{w}) \tag{3.12}$$

we can use (3.7) and (3.8) to simplify (3.10) and (3.11). The variation of $F_n - F_0$ as a function of $3Ksq_{\parallel}/2$ is shown schematically in figure 4. If the reduced free-energy difference between two phases is less than $O(\tilde{w}^2 w^{-2})$, then the stable phase cannot be identified because of higher-order terms in the expansion. Keeping this in mind, it is apparent from figure 4 that phases with $n \geq 2$ are degenerate for all $3Ksq_{\parallel}/2$, and that for

$$3Ksq_{\parallel}/2 > O(\tilde{w}) \tag{3.13}$$

one of these phases is stable. For

$$3Ksq_{\parallel}/2 \sim O(\tilde{w}) \tag{3.14}$$

a phase with $n \geq 1$ is stable, and for

$$3Ksq_{\parallel}/2 \sim O(\tilde{w}^2 w^{-2}) \tag{3.15}$$

all phases, $n \geq 0$, are degenerate at first order.

It also follows that for negative s such that

$$|3Ksq_{\parallel}/2| \geq O(\tilde{w}) \tag{3.16}$$

$n = 0$ is stable. Hence there is a transition from $n = 0$ to a phase with $n \geq 1$ in the region

$$-3Ksq_{\parallel}/2 \leq O(\tilde{w}) \qquad 3Ksq_{\parallel}/2 \leq O(\tilde{w}^2 w^{-2}). \tag{3.17}$$

Note that if $n = 1$ is shown to be stable in the region defined in (3.17), then it immediately follows from (3.13) that there is another transition to a phase with $n \geq 2$ in the region defined by (3.14).

The above equations depend on $\tilde{x}$, $\tilde{y}$ and $\tilde{w}$, but not on the coordination number of the lattice. Therefore the first-order results remain unaltered in the mean-field limit.

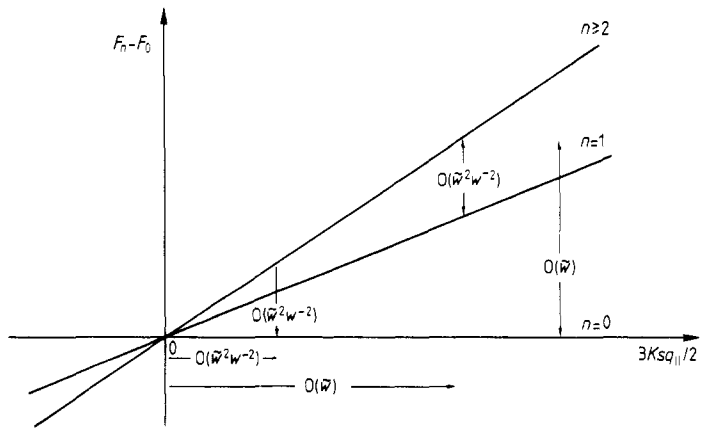

Figure 4. Reduced free-energy differences, $F_n - F_0$, $n \geq 1$, from first-order low-temperature series calculations.

3.2. Second order

The first-order calculations indicate that, to find an expression for the phase boundaries and determine the stability of interface phases with different values of n, requires consideration of terms in the expansion of at least $O(\tilde{w}^2)$. The number of ways of obtaining a given diagram, as well as its Boltzmann weight, now depends on $q_{\parallel}$ and $q_{\perp}$ as shown by the examples in appendix 1. A plot of $F_n - F_0$, $n \geq 1$, against $3Ksq_{\parallel}/2$ is shown in figure 5. It is important to remember that if the difference in free energies is less than $O(\tilde{w}^3 w^{-2})$ then the ordering of the phases may be altered by higher-order terms in the expansion. Phases with $n \geq 3$ are degenerate everywhere, and one of these phases is stable for large enough $3Ksq_{\parallel}/2$. For $3Ksq_{\parallel}/2 \sim O(\tilde{w})$ all $n \geq 2$ are degenerate, but second-order terms have broken the degeneracy between these phases and $n = 1$. In this region the contribution to the reduced free energy from second-order diagrams, together with using (3.7) and (3.8) to expand the terms in (3.10), leads to

$$F_1 - F_n = -3Ksq_{\parallel}(1-\tilde{x}^3)\tilde{w} + (1-\tilde{x}^3)^2[q_{\perp}w^{-1} - (q_{\perp}+1)]\tilde{w}^2 + O(\tilde{w}^3 w^{-2}) \qquad n \geq 2. \tag{3.18}$$

Hence there is a $1:n$, $n \geq 2$, boundary at

$$(3Ksq_{\parallel}/2)_{1:n} = \tfrac{1}{2}(1-\tilde{x}^3)[q_{\perp}(w^{-1}-1) - 1]\tilde{w} + O(\tilde{w}^2 w^{-2}) \qquad n \geq 2. \tag{3.19}$$

As the phase with $n = 1$ is stable there must be a $0:1$ boundary. This is given by

$$(3Ksq_{\parallel}/2)_{0:1} = (1-\tilde{x}^3)^2[q_{\perp}(w^{-1}-1) - 1]\tilde{w}^2 + \tfrac{1}{2}q_{\parallel}[(1-\tilde{x}^3)^2 + x^3 - 2 + \tilde{x}^3 x^{-3}(2-\tilde{x}^3)]\tilde{w}^2 + O(\tilde{w}^3 w^{-2}). \tag{3.20}$$

To take the mean-field limit, notice that we can write

$$w^{-1} = \exp[-\ln(\tilde{w})/q_{\perp}]. \tag{3.21}$$

Hence

$$q_{\perp}(w^{-1}-1) = q_{\perp}[-\ln(\tilde{w})/q_{\perp} + O(q_{\perp}^{-2})]. \tag{3.22}$$

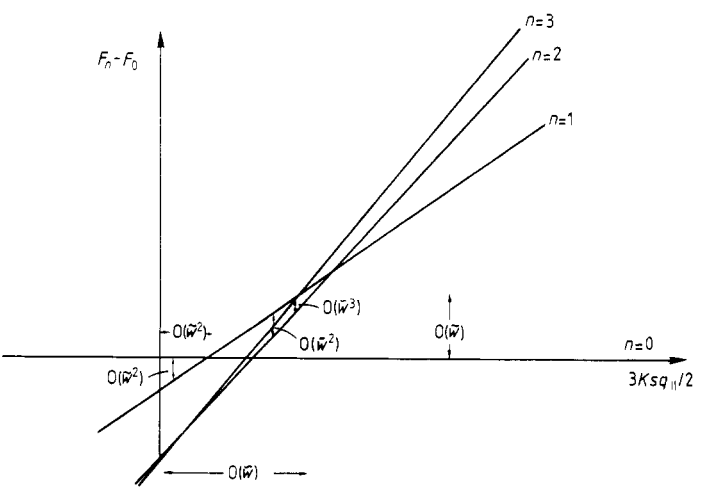

Figure 5. Reduced free-energy difference, $F_n - F_0$, $n \geq 1$, from second-order low-temperature series calculations.

Therefore, taking $q_\perp \to \infty$, $\tilde{w}$ = constant,

$$q_\perp(w^{-1}-1)-1 \to -[\ln(\tilde{w})+1]. \tag{3.23}$$

For temperatures within the ferromagnetic region the sign of $q_\perp(w^{-1}-1)-1$ does not change as $q_\perp$ is increased, although its magnitude is decreased. Therefore taking the mean-field limit at second order does not change the phase sequence but the boundaries are shifted to

$$(3Ksq_\parallel/2)^{\mathrm{mf}}_{0:1} = (1-\tilde{x}^3)^2[\ln(\tilde{x}^3)-\ln(\tilde{w})-1]\tilde{w}^2+O(\tilde{w}^3) \tag{3.24}$$

$$(3Ksq_\parallel/2)^{\mathrm{mf}}_{1:n} = -\tfrac{1}{2}(1-\tilde{x}^3)[\ln(\tilde{w})+1]\tilde{w}+O(\tilde{w}^2) \qquad n \geqslant 2. \tag{3.25}$$

So far changing $q_\parallel$ has had no effect on the phase diagram. Note, however, from (3.23), that both in-layer connected and disconnected diagrams are needed and contribute equally to the free-energy differences in the mean-field limit, whereas for finite $q_\perp$ terms arising from disconnections are $O(w)$ smaller.

3.3. Third order

The calculation needed to show that the mean-field limit does differ from the results for the simple cubic lattice is $F_2 - F_n$, $n \geqslant 3$, to third order. The sign of this free-energy difference along the $1:n$ boundary determines whether $n = 2$ appears as the next stable phase. The terms in the series become considerably more complicated, and many of the counting factors cannot be determined without a precise knowledge of the lattice structure. However, it is found that, in the region of interest, these factors combine such that an explicit expression can be found. Further description of the method of counting the diagrams is given in appendix 1.

For $3Ksq_\parallel/2 \sim O(\tilde{w})$ the expression for $F_2 - F_n$ is

$$\begin{aligned} F_2 - F_n = {} & -3Ksq_\parallel/2(1-\tilde{x}^3)[(1-\tilde{x}^3)+q_\parallel(x^{-3}-1)\tilde{x}^3]\tilde{w}^2 \\ & + q_\parallel(x^{-3}-1)\tilde{x}^3(1-\tilde{x}^3)^2[q_\perp(w^{-1}-1)-1]\tilde{w}^3 \\ & + O(\tilde{w}^4 w^{-2}) \qquad n > 2. \end{aligned} \tag{3.26}$$

Along the $1:n$ boundary, given by (3.19), (3.26) becomes

$$\begin{aligned} F_2 - F_n = {} & -\tfrac{1}{2}(1-\tilde{x}^3)^2[q_\perp(w^{-1}-1)-1][1-\tilde{x}^3-q_\parallel(x^{-3}-1)\tilde{x}^3]\tilde{w}^3 \\ & + O(\tilde{w}^4 w^{-2}) \qquad n > 2 \end{aligned} \tag{3.27}$$

which in the mean-field limit reduces to

$$(F_2 - F_n)^{\mathrm{mf}} = \tfrac{1}{2}(1-\tilde{x}^3)^2[1+\ln(\tilde{w})][(1-\tilde{x}^3)+2\tilde{x}^3\ln(\tilde{x}^3)]\tilde{w}^3+O(\tilde{w}^4) \qquad n > 2. \tag{3.28}$$

This is negative for temperatures such that

$$1+\ln(\tilde{w}) < 0+O(\tilde{w}) \tag{3.29}$$

and

$$1-\tilde{x}^3+2\tilde{x}^3\ln(\tilde{x}^3) > 0+O(\tilde{w}). \tag{3.30}$$

First we shall confine ourselves to discussing temperatures which satisfy the inequalities (3.29) and (3.30), as this range describes the region in the phase diagram where the results from the leading-order terms in a low-temperature expansion are most accurate.

Because (3.28) is negative $n=2$ does not appear as the next stable phase. We have not shown that the next stable phase in the mean-field limit is $n=\infty$; for this we need general-order diagrams whose contributions are calculated in § 3.4. First, however, we discuss the somewhat cumbersome expressions (3.26)-(3.28), which have been written down because they demonstrate the change in important fluctuations as $q_{\parallel}$ and $q_{\perp}$ are varied.

In equation (3.26) we have separated the contributions into those from second-order diagrams, i.e. axial chains and their disconnections across two adjacent layers as shown in figure 6(a), and third-order diagrams, i.e. similar chains but with extra 'kinks' or 'bumps' as shown in figure 6(b). For $3Ksq_{\parallel}/2 \sim O(w^{q_{\perp}})$, the sign of $F_2 - F_n$ is determined by the relative magnitude of these two terms. Note that varying the coordination numbers, $q_{\parallel}$ and $q_{\perp}$, does not cause their respective signs to change.

Now we examine (3.27) which gives the value of $F_2 - F_n$ along the $1:n$ boundary, within the temperature range specified by (3.29) and (3.30). Note that changing $q_{\perp}$ does not cause a change in sign of this free-energy difference. Hence, as found in § 3.2, altering the in-layer coordination number only changes the quantitative nature of the phase diagram. However, increasing $q_{\parallel}$ from $q_{\parallel}=2$ at fixed temperature causes the sign of (3.27) to change from positive to negative. Therefore, although the phase with $n=2$ appears as stable for $q_{\parallel}>2$, it does so at a non-zero temperature. As $q_{\parallel}$ increases, higher temperatures are required for the appearance of $n=2$ as a stable phase—the temperature above which it becomes stable is determined by

$$\tilde{x}^3 - 1 + q_{\parallel}(x^{-3} - 1)\tilde{x}^3 > 0 + O(\tilde{w}). \tag{3.31}$$

Increasing $q_{\parallel}$ reduces the contribution to the reduced free-energy difference of the third-order diagrams shown in figure 6(b). It is just these diagrams which stabilise the layering transitions: the simple axial chains shown in figure 6(a) always act repulsively between the the interfaces for $3Ksq_{\parallel}/2 > 0$.

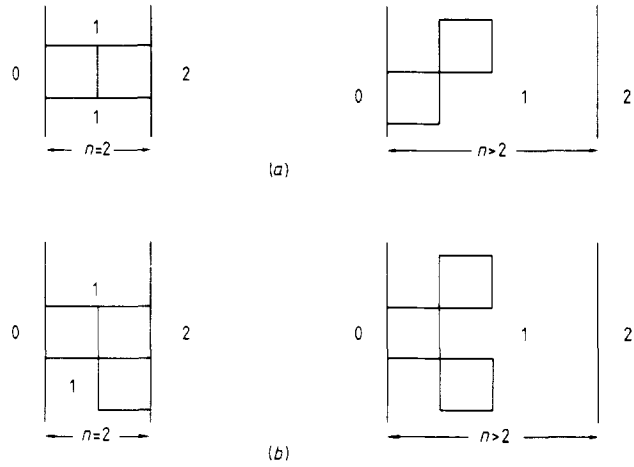

Figure 6. Examples of diagrams which contribute to $F_n - F_2$, $n>2$, for $3Ksq_{\parallel}/2 \sim O(w^{q_{\perp}})$ at third order. The blocks enclose flipped spins. (a) Axial chains and disconnections of two-spin flips. (b) As in (a) with an extra in-layer spin flip.

3.4. General order

Third-order calculations have been sufficient to show that $n = 2$ is not a stable phase at low temperatures for arbitrary coordination number. To demonstrate a $1:n$ phase boundary, where n is very large and possibly infinite, requires a general-order calculation.

The calculation of the leading-order terms in $F_n - F_{n'}$, $n' > n$, for arbitrary $q_\parallel$ and $q_\perp$ is considerably more complex than that in the previous papers of this series (Armitstead and Yeomans 1987, 1988). The details of the calculation are given in appendix 2, where the contributions to the free energy from the important fluctuations are built up using transfer matrices. Simple axial chains of length n require a product of 2×2 matrices. In the vicinity of $3Ksq_\parallel/2 \sim O(\tilde{w})$ these give zero contribution to $O(\tilde{w}^n)$.

At the next order in the expansion the contribution from 'bump' and 'kink' diagrams, some examples of which are shown in figure 7, must also be included. This requires an 8×8 matrix. The elements of this matrix are lattice dependent, as for the third-order calculations described in § 3.3 and appendix 1. However, for $3Ksq_\parallel/2 \sim O(\tilde{w})$ it is possible to obtain the expression

$$\begin{aligned} F_n - F_{n'} = -3Ksq_\parallel/2(1-\tilde{x}^3)[\tfrac{1}{2}q_\parallel(x^{-3}-1)]^{n-2}\tilde{x}^{3(n-2)}[\tilde{x}^3 q_\parallel(x^{-3}-1) \\ +(n-1)(1-\tilde{x}^3)]\tilde{w}^n + n(1-\tilde{x}^3)^2[\tfrac{1}{2}q_\parallel(x^{-3}-1)]^{n-1}\tilde{x}^{3(n-1)} \\ \times[q_\perp(w^{-1}-1)-1]\tilde{w}^{(n+1)} + O(\tilde{w}^{n+2}). \end{aligned} \tag{3.32}$$

All phases with $n' \geq n+1$ remain degenerate to this order of the expansion.

The coefficient of $3Ksq_\parallel/2$ in (3.32) arises from using (3.7) and (3.8) in the contribution from axial chains of length n. These chains act repulsively between the interfaces for all positive s. For $3Ksq_\parallel/2 > O(\tilde{w})$ this term, by itself, is of leading order

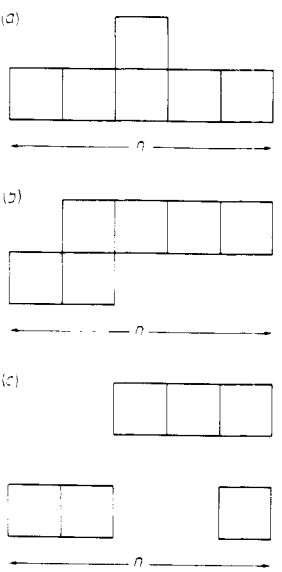

Figure 7. Some examples of 'bump' and 'kink' diagrams of length n, which contribute to $F_n - F_{n'}$, $n' > n$, for $3Ksq_\parallel/2 \sim O(\tilde{w})$ at leading order.

and, as it is negative, a phase with $n' > n$ is stable in this region. A similar consideration of $F_{n'} - F_{n+1}$, $n' > n+1$, at the next order of the expansion allows us to deduce that $n' > n+1$ is stable for $3Ksq_{\parallel}/2 > O(\tilde{w})$. Repeating this argument iteratively shows that for sufficiently large $3Ksq_{\parallel}/2$ a phase with very large n is stable. This term alone implies that $n = \infty$ is stable. However, for $n\tilde{w} \sim O(1)$ higher-order terms in the expansion may be important when determining the phase sequence.

For $3Ksq_{\parallel}/2 \sim O(\tilde{w})$ both of the terms in (3.32) contribute at the same order, $O(\tilde{w}^{n+1})$. The second term, from diagrams of length n with side 'kinks' and 'bumps', always acts attractively between the two interfaces, and, as in § 3.3, it is these fluctuations which stabilise any layering transitions.

To determine the next stable phase after $n = 1$, we examine the sign of $F_n - F_{n'}$, $n' > n$, along the $1:n$ boundary, given by (3.19). This gives

$$(F_n - F_{n'})_{1:n} = -\tfrac{1}{2}(1-\tilde{x}^3)^2(n-1)[1-\tilde{x}^3 - q_{\parallel}(x^{-3}-1)\tilde{x}^3] \times [\tfrac{1}{2}q_{\parallel}(x^{-3}-1)\tilde{x}^3]^{n-2}[q_{\perp}(w^{-1}-1)-1]\tilde{w}^{n+1} + O(\tilde{w}^{n+2}w^{-2}). \tag{3.33}$$

For temperatures below that given by (3.31), $T = T_1$ say, $F_n - F_{n'}$ is negative along the $1:n$ boundary. Hence a phase with $n' > n$ is stable along this boundary. Similar consideration of $F_{n+1} - F_{n'}$, $n' > n+1$, at next order in the expansion shows that the stable phase has $n' > n+1$. Repeating this argument recursively leads to a $1:n$ boundary, where n is very large and possibly infinite.

For temperatures above T_1 there is a $2:n$ boundary given, from (3.26), by

$$(3Ksq_{\parallel}/2)_{2:n} = \frac{q_{\parallel}(x^{-3}-1)\tilde{x}^3(1-\tilde{x}^3)[q_{\perp}(w^{-1}-1)-1]\tilde{w}}{1-\tilde{x}^3+q_{\parallel}(x^{-3}-1)\tilde{x}^3} + O(\tilde{w}^2w^{-2}). \tag{3.34}$$

In the same temperature region, $F_3 - F_n$, $n \geqslant 4$, is positive along the $2:n$, $n \geqslant 3$, boundary, from (3.32) and (3.34). Hence $n = 3$ is stable and we may use (3.32) to find the $3:n$, $n \geqslant 4$, boundary. It is straightforward to use an inductive argument as for the simple cubic model (Armitstead *et al* 1986) to demonstrate a sequence of layering transitions.

Figure 8 shows the phase diagram for finite, but arbitrary, $q_{\parallel}$ and $q_{\perp}$. All boundaries between phases with $n \geqslant 2$ meet at a point at finite temperature. However, this degeneracy may be lifted by higher-order terms in the expansion. Note that the $0:1$ boundary changes direction at sufficiently high temperature, as observed in figure 3.

In the mean-field limit the above results are qualitatively unchanged. Note, however, that the temperature T_1, above which we should expect to see layering transitions, is given, from (3.30), by $k_B T \geqslant Jq_{\parallel}$. The validity of the predictions from a low-temperature expansion is questionable at these temperatures, and the absence of a complete layering sequence in the numerical mean-field theory should not be surprising.

In table 1 we compare the predictions for the phase boundaries from the low-temperature limit of mean-field theory and a numerical solution of the mean-field equations for $J = J_0$. As expected, the differences are small, but increase with increasing temperature.

4. Discussion

We first briefly mention other work which is relevant to that discussed in this paper. Szpilka and Fisher (1986) studied the bulk phase diagram of the chiral clock model

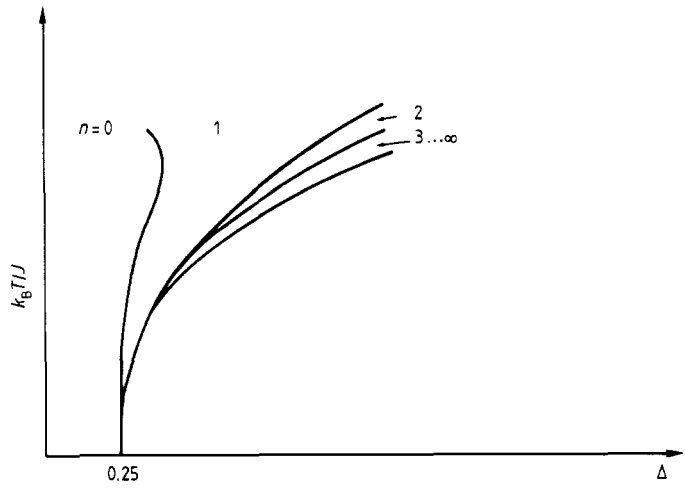

Figure 8. Qualitative interface phase diagram for finite coordination number.

for arbitrary coordination number using low-temperature series and found that here too the results depend on the coordination number. However, the important fluctuations are not the same as those for the interface problem.

Note also that Szpilka and Fisher (1986) have shown that the low-temperature series can be recast in a way which emphasises that the leading-order terms in the expansion can be interpreted as the interaction between interfaces. Although this does not give any new results, it provides a more physical way of understanding the significance of the terms in the free-energy difference.

We have made no mention of correction terms, other than to note that for $nw^{q_-^{-2}} \sim$ O(1) axial chains with several kinks and bumps will be important, and these correction terms must be considered in determining the phase sequence. We cannot therefore deduce an infinite sequence of layering transitions, nor indeed that the maximum value of n is ∞. This point is expanded further by Szpilka (1985).

We conclude by summarising the main results of this and the preceding two papers in the series. Our aim has been to show that low-temperature series expansions provide a useful alternative to mean-field theory in the study of interface phase transitions.

Table 1. A comparison of the phase boundaries, $\delta = \Delta - \frac{1}{4}$, obtained using a numerical solution of the mean-field equations and low-temperature series in the limit of infinite coordination number.

	Numerical solution of the mean-field equations		Low-temperature series in the mean-field limit	
k_BT/J_0	0:1	1:∞	0:1	1:∞
0.5	1.9×10^{-11}	2.4×10^{-6}	1.7×10^{-11}	2.7×10^{-6}
1.0	2.2×10^{-7}	9.4×10^{-4}	2.0×10^{-7}	9.2×10^{-4}
1.5	9.8×10^{-5}	6.5×10^{-3}	6.7×10^{-4}	5.3×10^{-3}
2.0	5.8×10^{-4}	1.8×10^{-2}	2.9×10^{-4}	1.2×10^{-2}

The two approaches usually, but not invariably, give qualitatively similar phase diagrams. The low-temperature series approach enables the fluctuations important in driving the phase transition to be pinpointed.

We first considered an interface in a q-state Potts model bound to the surface by a bulk field. Using both low-temperature and high-q expansions it was possible to show that for all q the interface unbound from the surface through a large, possibly infinite, number of first-order phase transitions as coexistence was approached. The width of successive phases decreased exponentially with the distance of the interface from the surface. The important fluctuations were linear chains of flipped spins stretching from the interface to the surface.

We then went on to consider solid-on-solid models where the interface was bound to the surface by a short-range pinning potential. We showed that again unbinding occurs through an infinite sequence of first-order transitions as the pinning potential tends to zero. Important fluctuations are now much more complicated than simple axial chains and hence higher-order terms in the expansion had to be considered to establish the phase sequence. This explained why it was difficult to establish an infinite sequence of layering transitions in the Abraham model (Duxbury and Yeomans 1985).

Finally, in this paper, we have considered the interface wetting transition in the three-state chiral clock model. We have shown that the mean-field results do not agree with the low-temperature expansions. In the former case the system has only two layering transitions, whereas in the latter there is a large, possibly infinite, number for a simple cubic lattice. This discrepancy is explained by calculating the dependence of the low-temperature series on lattice coordination number, and occurs because mean-field theory underestimates the effects of more complicated fluctuations. We show that as the coordination number is increased above that pertaining to a cubic lattice new phases appear at finite temperatures.

Acknowledgments

We should like to thank H U Everts and M Siegert for interesting discussions concerning their related work, and M E Fisher, A M Szpilka and A Lin for helpful communication.

Appendix 1

This appendix is devoted to an outline of the derivation of (3.18) and (3.26), with emphasis on the way in which arbitrary coordination number affects the terms in the low-temperature expansion. First two spin-flip diagrams, which contribute to both of these equations, are considered.

In table 2 we list the two spin-flip diagrams which contribute to $F_1 - F_n$, $n \geqslant 2$, together with their Boltzmann weights and counting factors per in-layer spin—these describe the difference in the number of ways such a diagram may be placed on the lattices (Fisher and Selke 1981). Because of the linked cluster theorem it is only necessary to quote the part linear in the number of in-layer spins, and hence m disconnections in a diagram contribute a coefficient of $(-1)^m$. To help understand the derivation of the terms in the table, figure 9 demonstrates the way in which arbitrary axial coordination number affects the Boltzmann weights. For each diagram there are

Table 2. Contribution to $F_1 - F_n$, $n \geq 2$, from two spin-flip diagrams. The spins flipped are shown in italics, and a bar between two spins indicates that they are disconnected.

Diagram	Count per in-layer spin	Boltzmann weight
$0\mathit{001}$	$-q_{\parallel}$	$(x^{q_{\parallel}/2-1}y^{q_{\parallel}/2-1} + xy^{3q_{\parallel}/2-2} + x^{q_{\parallel}/2-2}y^{q_{\parallel}/2+1} + x^{-1}y^{3q_{\parallel}/2-1})w^{2q_-}$
$0\mathit{0}\vert\mathit{01}$	$q_{\parallel}$	$2(x^{q_{\parallel}/2}y^{q_{\parallel}/2} + y^{3q_{\parallel}/2})w^{2q_\perp}$
$0\mathit{012}$	$q_{\parallel}$	$(x^{-q_{\parallel}+2}y^{q_{\parallel}/2-1} + x^{-q_{\parallel}+1}y^{q_{\parallel}/2+1} + x^{-3q_{\parallel}/2+1}y^{3q_{\parallel}/2-2} + x^{-3q_{\parallel}/2+2}y^{3q_{\parallel}/2-1})w^{2q_-}$
$0\mathit{0}\vert\mathit{12}$	$-q_{\parallel}$	$2(x^{-q_{\parallel}}y^{q_{\parallel}/2} + x^{-3q_{\parallel}/2}y^{3q_{\parallel}/2})w^{2q_-}$
$0\mathit{011}$	$-q_{\parallel}$	$(xy + 2x^{-q_{\parallel}/2+2}y^{q_{\parallel}-1} + x^{-q_{\parallel}+1}y^{2q_{\parallel}-2})w^{2q_-}$
$0\mathit{0}\vert\mathit{11}$	$q_{\parallel}$	$(1 + x^{-q_{\parallel}/2}y^{q_{\parallel}})^2 w^{2q_-}$
$0\mathit{000}$	$q_{\parallel}$	$(2x^{q_{\parallel}-1}y^{q_{\parallel}-1} + x^{q_{\parallel}+1}y^{q_{\parallel}-2} + x^{q_{\parallel}-2}y^{q_{\parallel}+1})w^{2q_-}$
$0\mathit{0}\vert\mathit{00}$	$-q_{\parallel}$	$4(x^{q_{\parallel}}y^{q_{\parallel}})w^{2q_-}$
$0\mathit{01}$ $0\mathit{01}$	$-q_-$	$(1 + x^{-q_{\parallel}}y^{2q_{\parallel}})w^{2q_--2} + 2(x^{-q_{\parallel}/2}y^{q_{\parallel}})w^{2q_--1}$
$0\underline{0}\mathit{1}$ $0\mathit{01}$	$(q_- + 1)$	$(1 + x^{-q_{\parallel}/2}y^{q_{\parallel}})^2 w^{2q_-}$
$0\mathit{12}$ $0\mathit{12}$	$q_\perp/2$	$2(x^{-2q_{\parallel}}y^{q_{\parallel}})w^{2q_--2} + 2(x^{-2q_{\parallel}}y^{q_{\parallel}})w^{2q_--1}$
$0\underline{1}\mathit{2}$ $0\mathit{12}$	$-(q_\perp + 1)/2$	$4(x^{-2q_{\parallel}}y^{q_{\parallel}})w^{2q_-}$
$0\mathit{00}$ $0\mathit{00}$	$q_\perp/2$	$2(x^{q_{\parallel}}y^{q_{\parallel}})w^{2q_--2} + 2(x^{q_{\parallel}}y^{q_{\parallel}})w^{2q_--1}$
$0\mathit{00}$ $0\bar{0}\mathit{0}$	$-(q_- + 1)/2$	$4(x^{q_{\parallel}}y^{q_{\parallel}})w^{2q_-}$

2^2 possible different combinations of final spin states. Note that the counts for axial diagrams depend on $q_{\parallel}$, whilst those for in-layer diagrams depend on $q_\perp$.

Adding the terms in table 2 gives the contribution to $F_1 - F_n$, $n \geq 2$, from two spin-flip diagrams, $(F_1 - F_n)_2$. For small $3Ksq_{\parallel}/2$ we may use (3.7) and (3.8) to expand y in terms of x, giving to leading order

$$(F_1 - F_n)_2 = (1 - \tilde{x}^3)^2[q_\perp w^{-1} - (q_\perp + 1)]\tilde{w}^2 + O(\tilde{w}^2 3Ksq_{\parallel}/2) \qquad n \geq 2 \qquad \text{(A1.1)}$$

as in the second term of (3.18).

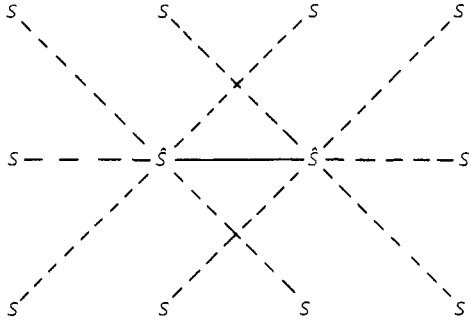

Figure 9. The effect of arbitrary axial coordination number (here $q_{\parallel} = 6$) on a chain of flipped spins. Layers are denoted by columns of spins, *S*. In each layer one spin (marked by a caret) is flipped. It is coupled to a neighbouring flipped spin by a full bond, and to unflipped spins by broken bonds. In-layer bonds are not shown.

In a similar way, table 3 contains a list of the contributions to $F_2 - F_n$, $n \geq 3$, from two spin-flip diagrams, $(F_2 - F_n)_2$. The leading-order term for small $3Ksq_\parallel/2$ is

$$(F_2 - F_n)_2 = -3Ksq_\parallel/2(1-\tilde{x}^3)[1-\tilde{x}^3 + q_\parallel(x^{-3}-1)\tilde{x}^3]\tilde{w}^2 + O(\tilde{w}^2(3Ksq_\parallel/2)^2) \qquad n \geq 3 \tag{A1.2}$$

as in the first term of (3.26). For $3Ksq_\parallel/2 \sim O(\tilde{w})$ the contribution from diagrams with three spin flips is of the same order as the leading term in $(F_2 - F_n)_2$ and therefore must also be considered. The counts for these diagrams not only depend on the coordination numbers, $q_\parallel$ and $q_\perp$, as for the two spin-flip diagrams listed in tables 2 and 3, but also on the connectivity of the lattice.

First we consider the contribution from 'dog-leg' diagrams where two connected in-layer spins both flip to the same state. These diagrams are listed in table 4(a). To avoid unduly complicated expressions for the Boltzmann weights, we have immediately put $y = x^2$ which from (3.7) and (3.8) will give a leading contribution $O(\tilde{w}^3 w^{-2})$ for $3Ksq_\parallel/2 \sim O(\tilde{w})$.

The pairs of spins in the same layer may be connected to the flipped spin in the adjacent layer by two, one or zero bonds. Therefore, in order to count the diagrams we define $c_{2,(1),(0)}$ which counts, for each orientation of in-layer connected spins, the number of ways of obtaining the diagram per in-layer spin, such that there are two, (one), (zero) axial bonds between flipped spins. Only that part linear in the number of in-layer spins is retained in the table, and hence a negative sign has been incorporated into the counts to allow for a disconnection (Fisher and Selke 1981). A little thought shows that

$$c_2 + c_1 = c_0. \tag{A1.3}$$

Adding the contributions in table 4(a), using (A1.3), gives a contribution to the reduced free-energy difference from three spin-flip diagrams,

$$(F_2 - F_n)_3 = 0 + O(\tilde{w}^3 w^{-1}) \qquad n \geq 3. \tag{A1.4}$$

The contribution $O(\tilde{w}^3 w^{-1})$ also arises from 'dog-leg' diagrams, but with the in-layer connected spins flipping to different states. The contributions to $F_2 - F_n$, $n \geq 3$, from such diagams are listed in table 4(b). Using (A1.3) gives

$$(F_2 - F_n)_3 = q_\perp(c_1 + 2c_2)\tilde{x}^3(x^{-3}-1)(1-\tilde{x}^3)^2\tilde{w}^3 w^{-1} + O(\tilde{w}^3) \qquad n \geq 3. \tag{A1.5}$$

Table 3. Contribution to $F_2 - F_n$, $n \geq 3$, from two spin-flip diagrams. The spins flipped are shown in italics, and a line between two spins indicates that they are disconnected.

Diagram	Count per in-layer spin	Boltzmann weight
0001	$-q_\parallel$	$(x^{q_\parallel/2-1}y^{q_\parallel/2-1} + xy^{3q_\parallel/2-2} + x^{-1}y^{3q_\parallel/2-1} + x^{q_\parallel/2-2}y^{q_\parallel/2+1})w^{2q_-}$
00|01	$q_\parallel$	$2(x^{q_\parallel/2}y^{q_\parallel/2} + y^{3q_\parallel/2})w^{2q_-}$
0112	$q_\parallel/2$	$(2x^{-q_\parallel/2-1}y^{q_\parallel-1} + x^{-2}y + x^{-q_\parallel+1}y^{2q_\parallel-2})w^{2q_-}$
01|12	$-q_\parallel/2$	$(1 + x^{-q_\parallel/2}y^{q_\parallel})^2 w^{2q_-}$
0000	$q_\parallel/2$	$(2x^{q_\parallel-1}y^{q_\parallel-1} + x^{q_\parallel+1}y^{q_\parallel-2} + x^{q_\parallel-2}y^{q_\parallel+1})w^{2q_-}$
00|00	$-q_\parallel/2$	$4(x^{q_\parallel}y^{q_\parallel})w^{2q_-}$

Table 4. Contribution to $F_2 - F_n$, $n \geq 3$, with $y = x^2$. Flipped spins are shown in *italics* and a bar between two spins indicates that they are disconnected. The notation c_i, d_i, $i = 0, 1, 2$, is defined in the text.

(*a*) Contribution at $O(w^{3q_- - 2})$.

Diagram	Count per in-layer spin	Boltzmann weight
0*0*0*0*	$2c_1 q_\perp/2$	$(3x^{9q_\parallel/2-3} + x^{9q_\parallel/2})w^{3q_- - 2}$
0*0*0*0*	$2c_2 q_\perp/2$	$(3x^{9q_\parallel/2-6} + x^{9q_\parallel/2})w^{3q_- - 2}$
	$-2c_0 q_\perp/2$	$4(x^{9q_\parallel/2})w^{3q_- - 2}$
0*0*0*1*	$-2c_1 q_\perp/2$	$(x^{3q_\parallel/2-3} + x^{3q_\parallel/2} + 2x^{9q_\parallel/2-3})w^{3q_- - 2}$
0*0*0*1*	$-2c_2 q_\perp/2$	$(x^{3q_\parallel/2-6} + x^{3q_\parallel/2} + 2x^{9q_\parallel/2-6})w^{3q_- - 2}$
	$2c_0 q_\perp/2$	$(2x^{3q_\parallel/2} + 2x^{9q_\parallel/2})w^{3q_- - 2}$
0*0*0*1*	$-2c_1 q_\perp/2$	$(x^{6q_\parallel/2-3} + x^{6q_\parallel/2} + 2x^{9q_\parallel/2-3})w^{3q_- - 2}$
0*0*0*1*	$-2c_2 q_\perp/2$	$(x^{6q_\parallel/2-6} + x^{6q_\parallel/2} + 2x^{9q_\parallel/2-6})w^{3q_- - 2}$
	$2c_0 q_\perp/2$	$(2x^{6q_\parallel/2} + 2x^{9q_\parallel/2})w^{3q_- - 2}$
0*1*1*2*	$2c_1 q_\perp/2$	$(1 + x^{3q_\parallel/2-3} + x^{6q_\parallel/2-3} + x^{9q_\parallel/2-3})w^{3q_- - 2}$
0*1*1*2*	$2c_2 q_\perp/2$	$(1 + x^{3q_\parallel/2-6} + x^{6q_\parallel/2-6} + x^{9q_\parallel/2-6})w^{3q_- - 2}$
	$-2c_0 q_\perp/2$	$(1 + x^{3q_\parallel/2} + x^{6q_\parallel/2} + x^{9q_\parallel/2})w^{3q_- - 2}$

(*b*) Contribution at $O(w^{3q_- - 1})$.

0*0*0*0*	$c_1 q_\perp$	$(3x^{9q_\parallel/2-3} + x^{9q_\parallel/2})w^{3q_- - 1}$
0*0*0*0*	$c_2 q_\perp$	$(2x^{9q_\parallel/2-3} + 2x^{9q_\parallel/2-6})w^{3q_- - 1}$
	$-c_0 q_-$	$(4x^{9q_\parallel/2})w^{3q_- - 1}$
0*0*0*1*	$-c_1 q_-$	$(3x^{6q_\parallel/2-3} + x^{6q_\parallel/2})w^{3q_- - 1}$
0*0*0*1*	$-c_2 q_-$	$(2x^{6q_\parallel/2-3} + 2x^{6q_\parallel/2-6})w^{3q_- - 1}$
	$c_0 q_-$	$(4x^{6q_\parallel/2})w^{3q_- - 1}$
0*0*0*1*	$-c_1 q_-$	$(x^{6q_\parallel/2-3} + x^{6q_\parallel/2} + 2x^{9q_\parallel/2-3})w^{3q_- - 1}$
0*0*0*1*	$-c_2 q_-$	$(2x^{6q_\parallel/2-3} + 2x^{9q_\parallel/2-6})w^{3q_- - 1}$
	$c_0 q_\perp$	$(2x^{6q_\parallel/2} + 2x^{9q_\parallel/2})w^{3q_- - 1}$
0*1*1*2*	$c_1 q_\perp$	$(x^{3q_\parallel/2-3} + x^{3q_\parallel/2} + 2x^{6q_\parallel/2-3})w^{3q_- - 1}$
0*1*1*2*	$c_2 q_-$	$(2x^{3q_\parallel/2-3} + 2x^{6q_\parallel/2-6})w^{3q_- - 1}$
	$-c_0 q_\perp$	$(2x^{3q_\parallel/2} + 2x^{6q_\parallel/2})w^{3q_- - 1}$

(*c*) Contribution from dog-leg diagrams at $O(w^{3q_-})$.

0*0*0*0*	$-d_1(q_\perp + 1)$	$(6x^{9q_\parallel/2-3} + 2x^{9q_\parallel/2})w^{3q_-}$
0*0*$\bar{0}$*0*	$-d_2(q_\perp + 1)$	$(5x^{9q_\parallel/2-6} + 2x^{9q_\parallel/2-3} + x^{9q_\parallel/2})w^{3q_-}$
	$d_0(q_\perp + 1)$	$(8x^{9q_\parallel/2})w^{3q_-}$
0*0*0*1*	$d_1(q_\perp + 1)$	$(x^{3q_\parallel/2-3} + x^{3q_\parallel/2} + x^{6q_\parallel/2} + 3x^{6q_\parallel/2-3} + 2x^{9q_\parallel/2-3})w^{3q_-}$
0*0*$\bar{0}$*1*	$d_2(q_\perp + 1)$	$(x^{3q_\parallel/2} + x^{3q_\parallel/2-6} + 2x^{6q_\parallel/2-6} + 2x^{6q_\parallel/2-3} + 2x^{9q_\parallel/2-6})w^{3q_\perp}$
	$-d_0(q_\perp + 1)$	$(2x^{3q_\parallel/2} + 4x^{6q_\parallel/2} + 2x^{9q_\parallel/2})w^{3q_-}$
0*0*0*1*	$d_1(q_\perp + 1)$	$(2x^{6q_\parallel/2} + 2x^{6q_\parallel/2-3} + 4x^{9q_\parallel/2-3})w^{3q_-}$
0*0*$\bar{0}$*1*	$d_2(q_\perp + 1)$	$(2x^{6q_\parallel/2-3} + x^{6q_\parallel/2-6} + x^{6q_\parallel/2} + 4x^{9q_\parallel/2-6})w^{3q_-}$
	$-d_0(q_\perp + 1)$	$(4x^{6q_\parallel/2} + 4x^{9q_\parallel/2})w^{3q_-}$
0*1*1*2*	$-d_1(q_\perp + 1)$	$(1 + 2x^{3q_\parallel/2-3} + x^{3q_\parallel/2} + 3x^{6q_\parallel/2-3} + x^{9q_\parallel/2-3})w^{3q_-}$
0$\bar{1}$*1*2*	$-d_2(q_\perp + 1)$	$(1 + x^{3q_\parallel/2-6} + 2x^{3q_\parallel/2-3} + 3x^{6q_\parallel/2-6} + x^{9q_\parallel/2-6})w^{3q_-}$
	$d_0(q_\perp + 1)$	$(1 + 3x^{3q_\parallel/2} + 3x^{6q_\parallel/2} + x^{9q_\parallel/2})w^{3q_-}$

Table 4. (continued)

Diagram	Count per in-layer spin	Boltzmann weight
(d) Contribution from axial chains at O(w^{3q_-}).		
00001	$-2(q_\parallel/2)^2$	$(x^{6q_\parallel/2-6}+3x^{9q_\parallel/2-6}+3x^{6q_\parallel/2-3}+x^{9q_\parallel/2-3})w^{3q_-}$
00|001	$2(q_\parallel/2)^2$	$(2x^{6q_\parallel/2-3}+2x^{6q_\parallel/2}+4x^{9q_\parallel/2-3})w^{3q_-}$
000|01	$2(q_\parallel/2)^2$	$(3x^{6q_\parallel/2-3}+x^{6q_\parallel/2}+3x^{9q_\parallel/2-3}+x^{9q_\parallel/2})w^{3q_-}$
00|0|01	$-2(q_\parallel/2)^2$	$(4x^{6q_\parallel/2}+4x^{9q_\parallel/2})w^{3q_-}$
00011	$-2(q_\parallel/2)^2$	$(x^{3q_\parallel/2}+x^{3q_\parallel/2+3}+3x^{6q_\parallel/2-3}+x^{6q_\parallel/2}+2x^{9q_\parallel/2-6})w^{3q_-}$
00|011	$2(q_\parallel/2)^2$	$(2x^{3q_\parallel/2+3}+4x^{6q_\parallel/2}+2x^{9q_\parallel/2-3})w^{3q_-}$
000|11	$2(q_\parallel/2)^2$	$(x^{3q_\parallel/2}+x^{3q_\parallel/2-3}+3x^{6q_\parallel/2-3}+x^{6q_\parallel/2}+2x^{9q_\parallel/2-3})w^{3q_-}$
00|0|11	$-2(q_\parallel/2)^2$	$(2x^{3q_\parallel/2}+4x^{6q_\parallel/2}+2x^{9q_\parallel/2})w^{3q_-}$
00112	$2(q_\parallel/2)^2$	$(x^3+x^{3q_\parallel/2-3}+2x^{3q_\parallel/2}+x^{6q_\parallel/2-6}+x^{9q_\parallel/2-6}+2x^{6q_\parallel/2-3})w^{3q_-}$
00|112	$-2(q_\parallel/2)^2$	$(1+2x^{3q_\parallel/2-3}+3x^{6q_\parallel/2-3}+x^{3q_\parallel/2}+x^{9q_\parallel/2-3})w^{3q_-}$
001|12	$-2(q_\parallel/2)^2$	$(x^3+2x^{3q_\parallel/2}+x^{6q_\parallel/2-3}+x^{3q_\parallel/2+3}+2x^{6q_\parallel/2}+x^{9q_\parallel/2-3})w^{3q_-}$
00|1|12	$2(q_\parallel/2)^2$	$(1+3x^{3q_\parallel/2}+3x^{6q_\parallel/2}+x^{9q_\parallel/2})w^{3q_-}$
00000	$2(q_\parallel/2)^2$	$(4x^{9q_\parallel/2-3}+4x^{9q_\parallel/2-6})w^{3q_-}$
00|000	$-2(q_\parallel/2)^2$	$(6x^{9q_\parallel/2-3}+2x^{9q_\parallel/2})w^{3q_-}$
000|00	$-2(q_\parallel/2)^2$	$(6x^{9q_\parallel/2-3}+2x^{9q_\parallel/2})w^{3q_-}$
00|0|00	$2(q_\parallel/2)^2$	$(8x^{9q_\parallel/2})w^{3q_-}$

This may be further simplified by noting that

$$c_1+2c_2=q_\parallel. \tag{A1.6}$$

Hence

$$(F_2-F_n)_3=q_\perp q_\parallel\tilde{x}^3(x^{-3}-1)(1-\tilde{x}^3)^2\tilde{w}^3w^{-1}+O(\tilde{w}^3) \qquad n\geq 3. \tag{A1.7}$$

For finite $q_\parallel$ and $q_\perp$ (A1.7) provides the leading-order term from three spin-flip diagrams for $3Ksq_\parallel/2\sim O(\tilde{w})$. However, for large $q_\parallel$ and $q_\perp$, $J_0q_\parallel$ and $Jq_\perp$ constant, the difference between $\tilde{w}^3w^{-1}$ and $\tilde{w}^3$ is very small, and vanishes in the mean-field limit, $q_\parallel$ and $q_\perp\to\infty$. Therefore we also need to include diagrams $O(\tilde{w}^3)$, which are three spin-flip diagrams having no connected in-layer flipped spins. These include both 'dog-leg' diagrams and connected and disconnected axial chains. The contributions from these diagrams are listed in tables 4(c) and (d), respectively. Analogous to the notation in tables 4(a) and (b), we have defined $d_{2,(1),(0)}$ to count, for each orientation of in-layer disconnected spins, the number of ways of obtaining the diagram per in-layer spin, such that there are two, (one), (zero) axial bonds between flipped spins.

Using

$$d_1+d_2=d_0 \tag{A1.8}$$

and

$$d_1+2d_2=q_\parallel \tag{A1.9}$$

we may add the contributions from tables 4(a)-(d) to obtain the leading-order term from all three spin-flip diagrams:

$$(F_2-F_n)_3=q_\parallel\tilde{x}^3(x^{-3}-1)(1-\tilde{x}^3)^2[q_\perp w^{-1}-(q_\perp+1)]\tilde{w}^3 + O(\tilde{w}^4w^{-1}) \qquad n\geq 3. \tag{A1.10}$$

Together with (A1.2), the contribution from two spin-flip diagrams, this gives equation (3.26).

Appendix 2

This appendix describes the matrices required to obtain (3.32). The diagrams which give the leading-order contribution to $F_{n'}-F_n$, $n'>n$, for $3Ksq_{\parallel}/2\sim O(\tilde{w})$ are axial chains of length n and their disconnections with possible 'kinks' and 'bumps': some examples are shown in figure 7. We use a transfer matrix method (Yeomans and Fisher 1984, Armitstead *et al* 1986) to build up such diagrams from left to right accounting at each step for the possibility that the chain might be broken and also allowing for the addition of two in-layer spins. The matrix elements are the Boltzmann factors contributed by the spin flips to the final spin states given by the labels on the rows and columns of the matrix.

The matrix products which must be considered have already been detailed in the appendices of Armitstead *et al* (1986) for the simple cubic model. Therefore we refer the reader to that paper for an explanation of the equations which we shall use, and here just extend the matrices published there to allow for arbitrary coordination number, and show how this affects the final results.

The matrix **M** which adds bonds between 0-0 layers may be written as

$$\mathbf{M}=\begin{array}{c} \underline{0\text{-}0} \\ \text{left spin} \end{array}\quad \begin{array}{c} \\ \text{right spin} \end{array}$$

$$\begin{array}{c|cccccccc} & 0 & 0 & 1 & 2 & 1 & \bar{1} & \bar{2} & \bar{2} \\ & 1 & 2 & 1 & 2 & 2 & \bar{1} & \bar{2} & \bar{1} \\ \hline 0\,1 & M_{11} & M_{12} & M_{13} & & & & & \\ 0\,2 & M_{21} & M_{22} & & \cdot & & & & \\ 1\,1 & M_{31} & & \cdot & & \cdot & & & \\ 2\,2 & \cdot & \cdot & & \cdot & & & & \\ 1\,2 & & & & & & & & \\ \bar{1}\,\bar{1} & \cdot & & & & & & & \\ \bar{2}\,\bar{2} & & & & & & & & \\ \bar{1}\,\bar{2} & \cdot & & & & & & & \end{array} \qquad \text{(A2.1)}$$

where a bar between two spins indicates that they are disconnected, and the matrix elements, M_{ij}, are listed in table 5. We have used the following notation.

k (l): the number of ways per in-layer spin that two in-layer connected spins may be joined to one spin in the previous layer such that there are two (one) axial bonds between the spins.

m (n): the number of ways per in-layer spin that two in-layer separated spins may be joined to one spin in the previous layer such that there are two (one) axial bonds between the spins.

k' (l'): the number of ways per in-layer spin that one spin may be joined to two connected spins in the previous layer such that there are two (one) axial bonds between the spins.

m' (n'): the number of ways per in-layer spin that one spin may be joined to two separated spins in the previous layer such that there are two (one) axial bonds between the spins.

Table 5. Elements of the matrix **M**, which adds bonds between 0-0 layers. The notation used is explained in appendix 2.

Matrix element	Value
M_{11}	$\frac{1}{2}q_{\parallel}(xy)^{q_{\parallel}/2}(x^{-1}y^{-1}-1)w^{q_{\perp}}$
M_{12}	$\frac{1}{2}q_{\parallel}y^{q_{\parallel}}(xy^{-2}-1)w^{q_{\perp}}$
M_{13}	$[kx^{q_{\parallel}-2}y^{q_{\parallel}/2-2}+lx^{q_{\parallel}-1}y^{q_{\parallel}/2-1}-(k+l)x^{q_{\parallel}}y^{q_{\parallel}/2}]w^{2q_{\perp}-2}$
M_{14}	$[kx^{2}y^{3q_{\parallel}/2-4}+lxy^{3q_{\parallel}/2-2}-(k+l)y^{3q_{\parallel}/2}]w^{2q_{\perp}-2}$
M_{15}	$[2kx^{q_{\parallel}/2}y^{q_{\parallel}-3}+l(x^{q_{\parallel}/2-1}y^{q_{\parallel}-1}+x^{q_{\parallel}/2+1}y^{q_{\parallel}-2})-2(k+l)x^{q_{\parallel}/2}y^{q_{\parallel}}]w^{2q_{\perp}-1}$
M_{16}	$-[mx^{q_{\parallel}-2}y^{q_{\parallel}/2-2}+nx^{q_{\parallel}-1}y^{q_{\parallel}/2-1}-(m+n)x^{q_{\parallel}}y^{q_{\parallel}/2}]w^{2q_{\perp}}$
M_{17}	$-[mx^{2}y^{3q_{\parallel}/2-4}+nxy^{3q_{\parallel}/2-2}-(m+n)y^{3q_{\parallel}/2}]w^{2q_{\perp}}$
M_{18}	$-[2mx^{q_{\parallel}/2}y^{q_{\parallel}-3}+n(x^{q_{\parallel}/2-1}y^{q_{\parallel}-1}+x^{q_{\parallel}/2+1}y^{q_{\parallel}-2})-2(m+n)x^{q_{\parallel}/2}y^{q_{\parallel}}]w^{2q_{\perp}}$
M_{21}	$\frac{1}{2}q_{\parallel}x^{q_{\parallel}}(x^{-2}y-1)w^{q_{\perp}}$
M_{22}	$\frac{1}{2}q_{\parallel}(xy)^{q_{\parallel}/2}(x^{-1}y^{-1}-1)w^{q_{\perp}}$
M_{23}	$[kx^{3q_{\parallel}/2-4}y^{2}+lx^{3q_{\parallel}/2-2}y-(k+l)x^{3q_{\parallel}/2}]w^{2q_{\perp}-2}$
M_{24}	$[kx^{q_{\parallel}/2-2}y^{q_{\parallel}-2}+lx^{q_{\parallel}/2-1}y^{q_{\parallel}-1}-(k+l)x^{q_{\parallel}/2}y^{q_{\parallel}}]w^{2q_{\perp}-2}$
M_{25}	$[2kx^{q_{\parallel}-3}y^{q_{\parallel}/2}+l(x^{q_{\parallel}-2}y^{q_{\parallel}/2+1}+x^{q_{\parallel}-1}y^{q_{\parallel}/2-1})-2(k+l)x^{q_{\parallel}}y^{q_{\parallel}/2}]w^{2q_{\perp}-1}$
M_{26}	$-[mx^{3q_{\parallel}/2-4}y^{2}+nx^{3q_{\parallel}/2-2}y-(m+n)x^{3q_{\parallel}/2}]w^{2q_{\perp}}$
M_{27}	$-[mx^{q_{\parallel}/2-2}y^{q_{\parallel}-2}+nx^{q_{\parallel}/2-1}y^{q_{\parallel}-1}-(m+n)x^{q_{\parallel}/2}y^{q_{\parallel}}]w^{2q_{\perp}}$
M_{28}	$-[2mx^{q_{\parallel}-3}y^{q_{\parallel}/2}+n(x^{q_{\parallel}-2}y^{q_{\parallel}/2+1}+x^{q_{\parallel}-1}y^{q_{\parallel}/2-1}-2(m+n)x^{q_{\parallel}}y^{q_{\parallel}/2}]w^{2q_{\perp}}$
M_{31}	$[k'x^{q_{\parallel}/2-2}y^{q_{\parallel}-2}+l'x^{q_{\parallel}/2-1}y^{q_{\parallel}-1}-(k'+l')x^{q_{\parallel}/2}y^{q_{\parallel}}]w^{q_{\perp}}$
M_{32}	$[k'x^{2}y^{3q_{\parallel}/2-4}+l'xy^{3q_{\parallel}/2-2}-(k'+l')y^{3q_{\parallel}/2}]w^{q_{\perp}}$
M_{41}	$[k'x^{3q_{\parallel}/2-4}y^{2}+l'x^{3q_{\parallel}/2-2}y-(k'+l')x^{3q_{\parallel}/2}]w^{q_{\perp}}$
M_{42}	$[k'x^{q_{\parallel}-2}y^{q_{\parallel}/2-2}+l'x^{q_{\parallel}-1}y^{q_{\parallel}/2-1}-(k'+l')x^{q_{\parallel}}y^{q_{\parallel}/2}]w^{q_{\perp}}$
M_{51}	$[k'x^{q_{\parallel}-3}y^{q_{\parallel}/2}+\frac{1}{2}l'(x^{q_{\parallel}-1}y^{q_{\parallel}/2-1}+x^{q_{\parallel}-2}y^{q_{\parallel}/2+1})-(k'+l')x^{q_{\parallel}}y^{q_{\parallel}/2}]w^{q_{\perp}}$
M_{52}	$[k'x^{q_{\parallel}/2}y^{q_{\parallel}-3}+\frac{1}{2}l'(x^{q_{\parallel}/2+1}y^{q_{\parallel}-2}+x^{q_{\parallel}/2-1}y^{q_{\parallel}-1})-(k'+l')x^{q_{\parallel}/2}y^{q_{\parallel}}]w^{q_{\perp}}$
M_{61}	$[m'x^{q_{\parallel}/2-2}y^{q_{\parallel}-2}+n'x^{q_{\parallel}/2-1}y^{q_{\parallel}-1}-(m'+n')x^{q_{\parallel}/2}y^{q_{\parallel}}]w^{q_{\perp}}$
M_{62}	$[m'x^{2}y^{3q_{\parallel}/2-4}+n'xy^{3q_{\parallel}/2-2}-(m'+n')y^{3q_{\parallel}/2}]w^{q_{\perp}}$
M_{71}	$[m'x^{3q_{\parallel}/2-4}y^{2}+n'x^{3q_{\parallel}/2-2}y-(m'+n')x^{3q_{\parallel}/2}]w^{q_{\perp}}$
M_{72}	$[m'x^{q_{\parallel}-2}y^{q_{\parallel}/2-2}+n'x^{q_{\parallel}-1}y^{q_{\parallel}/2-1}-(m'+n')x^{q_{\parallel}}y^{q_{\parallel}/2}]w^{q_{\perp}}$
M_{81}	$[m'x^{q_{\parallel}-3}y^{q_{\parallel}/2}+\frac{1}{2}n'(x^{q_{\parallel}-1}y^{q_{\parallel}/2-1}+x^{q_{\parallel}-2}y^{q_{\parallel}/2+1})-(m'+n')x^{q_{\parallel}}y^{q_{\parallel}/2}]w^{q_{\perp}}$
M_{82}	$[m'x^{q_{\parallel}/2}y^{q_{\parallel}-3}+\frac{1}{2}n'(x^{q_{\parallel}/2+1}y^{q_{\parallel}-2}+x^{q_{\parallel}/2-1}y^{q_{\parallel}-1})-(m'+n')x^{q_{\parallel}/2}y^{q_{\parallel}}]w^{q_{\perp}}$
M_{ij} $i,j\geq 3$	0

We mention the important points in the construction of the matrix **M**. Further comments which are also relevant for the simple cubic model may be found in Armitstead *et al* (1986). Note however, that the 8×8 matrix used there may in fact be reduced to a 5×5 matrix by combining the rows (columns) 1 with 3, 2 with 4, and 6 with 7.

(a) There are eight final states which must be considered. The reason for listing in-layer connections and disconnections separately is that the counting factors for

adding the next spin in the chain are different for the two cases. This was not so for the simple cubic model (Armitstead *et al* 1986), where they could be considered in the same row or column. Consequently, many of the Boltzmann weights occur in pairs, for example, M_{13} and M_{16}, M_{24} and M_{27}, etc.

(b) Only diagrams with at most one layer containing two flipped spins are required. Hence M_{ij}, $i, j \geqslant 3$, are of higher order and put equal to zero.

(c) Using relationships such as (A1.3) and (A1.8) we have substituted the counts for diagrams having no axial bonds between flipped spins by minus the sum of the counts for diagrams having two and one axial bonds between flipped spins.

(d) If two in-layer spins flip to different final states instead of the same final states, the number of diagrams is doubled. This is because of the loss in symmetry of the in-layer spins. The matrices in Armitstead *et al*(1986) explicitly displayed this symmetry by allowing for more final states. Hence, as noted above, there was an increase in the size of **M**.

The other matrix we shall need adds spins between 0-1 layers. It will become apparent that to the order considered we only need the elements which add a single spin. The relevant elements of this matrix, **N**, are therefore given by

$$\underline{0\text{-}1} \qquad \begin{matrix} & \begin{matrix} 1 \\ 2 \end{matrix} & \begin{matrix} 1 \\ 0 \end{matrix} \\ \begin{matrix} 0 \\ 1 \end{matrix} & \left[\begin{matrix} \tfrac{1}{2}q_{\parallel}(x^{-q_{\parallel}+2}y^{q_{\parallel}/2-1} - x^{-q_{\parallel}}y^{q_{\parallel}/2}) & \tfrac{1}{2}q_{\parallel}(x^{-q_{\parallel}+1}y - x^{-q_{\parallel}}) \\ \tfrac{1}{2}q_{\parallel}(x^{-q_{\parallel}+1}y^{q_{\parallel}-2} - x^{-q_{\parallel}}y^{q_{\parallel}}) & \tfrac{1}{2}q_{\parallel}(x^{-q_{\parallel}+2}y^{q_{\parallel}/2-1} - x^{-q_{\parallel}}y^{q_{\parallel}/2}) \end{matrix} \right] w^{q_-} \\ \begin{matrix} 0 \\ 2 \end{matrix} \end{matrix} \qquad \mathbf{N} = \qquad \text{(A2.2)}$$

The row vectors which add the initial bond between 0-0 and 0-1 layers, $\boldsymbol{M}_i$ and $\boldsymbol{N}_i$, respectively, are (written as their transposes)

$$\underline{0\text{-}0} \qquad \begin{matrix} & 0 \\ \begin{matrix} 0 \\ 1 \end{matrix} & \left[x^{q_{\parallel}/2}w^{q_-} \right] \\ \begin{matrix} 0 \\ 2 \end{matrix} & \left[y^{q_{\parallel}/2}w^{q_-} \right] \\ \begin{matrix} 1 \\ 1 \end{matrix} & \left[\tfrac{1}{2}q_{\perp}x^{q_{\parallel}}w^{2q_- -2} \right] \\ \begin{matrix} 2 \\ 2 \end{matrix} & \left[\tfrac{1}{2}q_{-}y^{q_{\parallel}}w^{2q_- -2} \right] \\ \begin{matrix} 1 \\ 2 \end{matrix} & \left[q_- x^{q_{\parallel}/2}y^{q_{\parallel}/2}w^{2q_- -1} \right] \\ \begin{matrix} \tfrac{1}{1} \end{matrix} & \left[-\tfrac{1}{2}(q_- +1)x^{q_{\parallel}}w^{2q_-} \right] \\ \begin{matrix} \tfrac{2}{2} \end{matrix} & \left[-\tfrac{1}{2}(q_- +1)y^{q_{\parallel}}w^{2q_-} \right] \\ \begin{matrix} \tfrac{1}{2} \end{matrix} & \left[-(q_- +1)x^{q_{\parallel}/2}y^{q_{\parallel}/2}w^{2q_-} \right] \end{matrix} \qquad \boldsymbol{M}_i^{\mathrm{T}} = \qquad \underline{0\text{-}1} \qquad \begin{matrix} & 0 \\ \begin{matrix} 1 \\ 2 \end{matrix} & \left[x^{-q_{\parallel}/2}y^{q_{\parallel}/2}w^{q_-} \right] \\ \begin{matrix} 1 \\ 0 \end{matrix} & \left[x^{-q_{\parallel}/2}w^{q_-} \right] \\ \begin{matrix} 2 \\ 2 \end{matrix} & \left[\tfrac{1}{2}q_{-}x^{-q_{\parallel}}y^{q_{\parallel}}w^{2q_- -2} \right] \\ \begin{matrix} 0 \\ 0 \end{matrix} & \left[\tfrac{1}{2}q_{\perp}x^{-q_{\parallel}}w^{2q_- -2} \right] \\ \begin{matrix} 2 \\ 0 \end{matrix} & \left[q_{\perp}x^{-q_{\parallel}}y^{q_{\parallel}/2}w^{2q_- -1} \right] \\ \begin{matrix} \tfrac{2}{2} \end{matrix} & \left[-\tfrac{1}{2}(q_- +1)x^{-q_{\parallel}}y^{q_{\parallel}}w^{2q_-} \right] \\ \begin{matrix} \tfrac{0}{0} \end{matrix} & \left[-\tfrac{1}{2}(q_- +1)x^{-q_{\parallel}}w^{2q_-} \right] \\ \begin{matrix} \tfrac{2}{0} \end{matrix} & \left[-(q_{\perp}+1)x^{-q_{\parallel}}y^{q_{\parallel}/2}w^{2q_-} \right] \end{matrix} \qquad \boldsymbol{N}_i^{\mathrm{T}} = \qquad \text{(A2.3)}$$

Finally, we need the column vectors which describe the final bond between 0-0 and 0-1 layers, $\boldsymbol{M}_f$ and $\boldsymbol{N}_f$, respectively

$$\boldsymbol{M}_f = \begin{array}{c|c} \underline{0\text{-}0} & 0 \\ \hline 0,1 & y^{q_\perp/2} \\ 0,2 & x^{q_\perp/2} \\ 1,1 & y^{q_\perp} \\ 2,2 & x^{q_\parallel} \\ 1,2 & x^{q_\perp/2}y^{q_\parallel/2} \\ \frac{1}{1} & y^{q_\perp} \\ \frac{2}{2} & x^{q_\perp} \\ \frac{1}{2} & x^{q_\perp/2}y^{q_\parallel/2} \end{array} \qquad \boldsymbol{N}_f = \begin{array}{c|c} \underline{0\text{-}1} & 1 \\ \hline 0,1 & x^{-q_\parallel/2} \\ 0,2 & x^{-q_\parallel/2}y^{q_\parallel/2} \\ 1,1 & x^{-q_\perp} \\ 2,2 & x^{-q_\perp}y^{q_\perp} \\ 1,2 & x^{-q_\parallel}y^{q_\parallel/2} \\ \frac{1}{1} & x^{-q_\perp} \\ \frac{2}{2} & x^{-q_\parallel}y^{q_\parallel} \\ \frac{1}{2} & x^{-q_\parallel}y^{q_\parallel/2} \end{array} \tag{A2.4}$$

The contribution to $F_n - F_{n'}$, $n' > n$, to order $O(\tilde{w}^{n+1})$ is given from (A1.9) and (A1.11) of Armitstead *et al* (1986) by

$$F_n - F_{n'} = 2(\boldsymbol{N}_i - \boldsymbol{M}_i)\mathbf{M}^{n-1}\mathbf{N}\boldsymbol{M}_f + 2\boldsymbol{M}_i\mathbf{M}^n(\boldsymbol{M}_f - \boldsymbol{N}_f) + (\boldsymbol{N}_i - \boldsymbol{M}_i)\mathbf{M}^{n-1}(\boldsymbol{N}_f - \boldsymbol{M}_f) \qquad n' > n. \tag{A2.5}$$

The first two terms are from axial chains of length $(n+1)$ and have a coefficient of $\tilde{w}^{n+1}$. Therefore, recalling that $3Ksq_\parallel/2 \sim O(\tilde{w})$, we may put $y = x^2$ in the matrix elements and put equal to zero any elements greater than $O(\tilde{w})$ to this order. **M** reduces to a 2×2 triangular matrix and the product may be performed to give

$$(\boldsymbol{N}_i - \boldsymbol{M}_i)\mathbf{M}^{n-1}\mathbf{N}\boldsymbol{M}_f + \boldsymbol{M}_i\mathbf{M}^n(\boldsymbol{M}_f - \boldsymbol{N}_f) = 0 + O(\tilde{w}^{n+2}). \tag{A2.6}$$

The final term in (A2.5) arises from axial chains of length n with possible kinks and bumps. The simple chains, i.e. diagrams with only one spin flipped in each layer, have a coefficient of $\tilde{w}^n$ and are described by the 2×2 matrix in the top left-hand corner of **M**. We must keep the full dependence of y upon x whilst evaluating this part of the product in (A2.5), which may be done by diagonalisation of the 2×2 matrix. Expanding y in terms of x in the final expression gives the leading-order contribution to $F_n - F_{n'}$, $n' > n$, from axial chains of length n:

$$-3Ksq_\parallel/2(1-\tilde{x}^3)[\tfrac{1}{2}q_\parallel(x^{-3}-1)\tilde{x}^3]^{n-2}[q_\parallel\tilde{x}^3(x^{-3}-1) + (n-1)(1-\tilde{x}^3)]\tilde{w}^n + O(\tilde{w}^{n+2}). \tag{A2.7}$$

The same approach, in principle, could also be applied to the full 8×8 matrix. However, as we are interested in, and indeed this matrix is only valid for, the leading-order term, it is simpler to put $y = x^2$ and explicitly evaluate the product of

the resulting sparse matrix, retaining only those terms which may contribute up to $O(\tilde{w}^{n+1})$. Using

$$2k+l=q_{\parallel}q_{\perp}/2 \qquad 2m+n=q_{\parallel}(q_{\perp}+1)/2 \tag{A2.8}$$

and

$$2k'+l'=q_{\parallel} \qquad 2m'+n'=q_{\parallel} \tag{A2.9}$$

this gives

$$n(1-\tilde{x}^3)^2[\tfrac{1}{2}q_{\parallel}(x^{-3}-1)]^{n-1}\tilde{x}^{3(n-1)}[q_{\perp}(w^{-1}-1)-1]\tilde{w}^{n+1}. \tag{A2.10}$$

Together with (A2.7) this leads to (3.32).

References

Armitstead K and Yeomans J M 1987 *J. Phys. A: Math. Gen.* **20** 5635
—— 1988 *J. Phys. A: Math. Gen.* **21** 159
Armitstead K, Yeomans J M and Duxbury P 1986 *J. Phys. A: Math. Gen.* **19** 3165
Duxbury P M and Yeomans J M 1985 *J. Phys. A: Math. Gen.* **18** L983
Fisher M E and Selke W 1981 *Phil. Trans. R. Soc.* **302** 1
Huse D A and Fisher M E 1984 *Phys. Rev.* B **29** 239
Ottinger H C 1982 *J. Phys. C: Solid State Phys.* **15** L1257
Szpilka A M 1985 *PhD thesis* Cornell University
Szpilka A M and Fisher M E 1986 *Phys. Rev. Lett.* **57** 1044
Thompson C J 1974 *Commun. Math. Phys.* **36** 225
Yeomans J M and Fisher M E 1984 *Physica* **127A** 1
Yokoi C S O, Coutinho-filho M D and Salinas S R 1981 *Phys. Rev.* B **24** 4047